

# Combining Finite Volume and Finite Element Methods to Simulate Fluid Flow in Geologic Media

Sebastian Geiger\*    Stephen Roberts<sup>†</sup>    Stephan K. Matthäi<sup>‡</sup>  
Christopher Zoppou<sup>§</sup>

1st September 2001

## Abstract

The permeability, porosity, and velocity that govern the flow of multi-phase fluids (e.g., water, oil, steam) in the earth's subsurface can vary over several orders of magnitude. The range over which the flow is observed can vary from the kilometre to centimetre scale due to the hydraulic properties and geometric complexity of geologic structures. Combining node-centred finite volumes with a finite element method on an unstructured triangular grid is an efficient way to accurately model multi-phase flow in geologic media. We demonstrate such a method by simulating multi-phase flow in geological media with complex geometries and transport parameters that vary over several orders of magnitude.

## Contents

|          |                            |          |
|----------|----------------------------|----------|
| <b>1</b> | <b>Introduction</b>        | <b>2</b> |
| <b>2</b> | <b>Governing Equations</b> | <b>5</b> |

---

\*Department of Earth Sciences, Swiss Federal Institute of Technology (ETH), Sonneggstr. 5, CH-8092 Zurich, SWITZERLAND.

<sup>†</sup>Department of Mathematics, School of Mathematical Sciences, Australian National University, Canberra, ACT 0200, AUSTRALIA.

<sup>‡</sup>TH Huxley School of Environment, Earth Science and Engineering, Imperial College, RSM Building, Prince Consort Road, London SW7 2BP, ENGLAND.

<sup>§</sup>Water Division, ACTEW Corporation, Canberra, ACT 2601, AUSTRALIA.

|          |  |          |
|----------|--|----------|
| <b>3</b> | <b>Numerical Method</b>  | <b>5</b> |
| 3.1      | Second-order Accuracy and Slope Limiters . . . . .                   | 6        |
| <b>4</b> | <b>Numerical Experiment: Two-phase Flow in a Fractured Reservoir</b> | <b>7</b> |
| <b>5</b> | <b>Conclusion and Outlook</b>  | <b>9</b> |

# 1 Introduction

Fluid flow in geological systems often involves the simultaneous propagation of multiple fluid phases (e.g., water-oil, water-steam) [11]. Modelling the flow of multi-phase fluids such as water, oil and steam in the earth’s crust is often challenging, since the hydrological rock properties (permeability, porosity) and the velocities can vary over several orders of magnitude. As a result, hydraulic conditions often focus large scale fluid flows (e.g., in a large oil reservoir) into much smaller volumes (e.g., fractures). In such cases the scale of interest can vary from the kilometre to centimetre scale [13], [14].

The combination of finite element and finite volume methods (hereafter called CEVM) to model multi-phase flow in geologic media has recently become popular (e.g., [6], [5], [3]). These studies have shown that CEVM simulations yield very good results compared to traditional finite difference or finite element methods [9]. The CEVM is commonly embedded within an implicit pressure explicit saturation formulation (IMPES). In the IMPES approach, the fluid pressure field is computed implicitly (here using the finite element method), yielding velocities of the fluid phases which are used to explicitly calculate the mass balance of the fluid phases (here using the finite volume method) [2]. The use of the CEVM and IMPES formulation combines the best features of either method. In particular:

- The geometric flexibility of the finite-element method is retained such that large variations in scale can be modelled efficiently.
- The non-linear advection equations can be decoupled from the parabolic equation for the fluid pressure, which in the case of incompressible fluids avoids the need for Newton like iterations.
- The parabolic equation for the fluid pressure can be solved efficiently by the finite element and the hyperbolic mass-conservation equation efficiently by the finite volume method.
- Algebraic multigrid solvers can be employed to solve the equations associated with the finite element method.

- Mass conservative, total variation diminishing (TVD) finite volume schemes can be used to accurately track the propagation of the phase interfaces.

When embedding the CEVM in an IMPES formulation, a mixed-element formulation is commonly used to simultaneously compute the fluid pressure and velocity fields at the finite element nodes (e.g., [6], [5], [3], [9]). This yields a flux that is constant across the faces of the finite elements. This method does not require the construction of a finite volume subgrid. However it has the major drawback that the physical solution across interfaces with discontinuous changes of material properties is incorrect [24]. Another disadvantage is that large matrices must be constructed, which increases the storage and CPU time required by the multigrid solvers.

Verma [23] has suggested that the use of node-centred (barycentric) finite volumes is well suited for reservoir simulation. In this method, a finite volume subgrid is constructed on the basis of a triangular in two dimensions (or tetrahedral in three dimensions) finite element mesh by connecting the barycentres of the triangles with the midpoints of the associated edges (Figure 1).

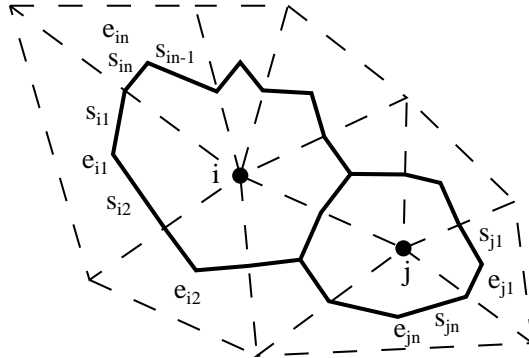


Figure 1: Barycentric (node-centered) finite volumes at nodes  $i$  and  $j$  with triangular finite elements  $e_{i1} - e_{in}$  ( $e_{j1} - e_{jn}$ , respectively) and segments  $s_{i1} - s_{in}$  ( $s_{j1} - s_{jn}$ , respectively) as defined in [23].

While the geometric flexibility of unstructured meshes is retained, this method has the advantage that only the fluid pressure field must be computed by the finite element method. In contrast to the mixed-element formulation, the transport parameters are now element variables, and element fluid velocities are derived from the fluid pressure field. This leads to a fluid flux that is constant across the segments of a finite volume within the associated finite element. Furthermore, with the transport parameters and fluid flux assigned to the finite elements, the contributions of the respective element fluid fluxes are averaged to the nodes such

that the fluid mass within the finite volume is conserved. Hence, the formulation can cope with large variations of the transport parameters and discontinuous changes of the material properties, because the fluid flux can vary from element to element. The drawback of this formulation is the construction and subsequent storage requirements, especially in 3D, of a finite volume subgrid. The feasibility of three different node-centered finite volume discretizations within the CEVM framework were discussed recently [10]. In that study, a mixed-element formulation and nodal transport parameters were used, which can lead to a failure of the algorithm if the mobility tensor becomes negative.

CEVM is usually applied to the numerical simulation of incompressible fluid phases. Recent studies indicate that CEVM can also be used to model the flow of compressible phases, [3], [19].

In CEVM, special attention is usually paid to the hyperbolic mass-conservation equation, which when neglecting dispersive terms, takes the basic form of the advection equation:

$$\frac{\partial u}{\partial t} + \nabla \cdot \mathbf{v}u = 0 \quad (1)$$

where  $u$  is the conserved quantity and  $\mathbf{v}$  is the velocity vector.

Due to its hyperbolic character, solutions of the advection equation are prone to numerical diffusion when using first order Godunov or Lax-Friedrichs methods or spurious oscillations when higher order Lax-Wendroff or Beam-Warming methods are used.

Several numerical methods have been developed in recent years that are capable of capturing the advective (shock) front accurately. Popular choices include approximate Riemann solvers (e.g., [18], [22]), TVD methods (e.g., [4], [21]), essentially non-oscillatory methods (ENO) (e.g., [7], [20]), and central schemes (e.g., [16], [12]). While all of these methods have been shown to be robust for numerous applications (e.g., [1], [25]), the TVD scheme is the most computationally efficient method when applied to a simple one-dimensional, linear conservation law such as the advection equation. Therefore, TVD methods are usually employed to solve the advection equation within the CEVM framework (e.g., [6], [5], [3], [9]). It was shown recently that TVD applied to the CEVM method generally yields very accurate solutions [9].

The paper is structured as follows: The governing equations for multi-phase flow in geologic media are discussed. This is followed by the description of the numerical method, the extension of the slope limited TVD method to barycentric finite volumes and unstructured grids. Finally we conduct a numerical experiment and apply the CEVM to a hypothetical example where oil is pumped out of a fractured reservoir.

## 2 Governing Equations

The equations describing the flow of two incompressible and immiscible fluids can be derived by combining Darcy's law and mass conservation written for each phase individually (e.g., [8]). Note that the reduction of the formulation to a single-phase fluid system is straightforward. The parabolic equation describing the fluid pressure  $p$  in the reservoir is defined as

$$c_t \phi \frac{\partial p}{\partial t} + \nabla \cdot \mathbf{v}_t = Q_t \quad (2)$$

where the velocity vector  $\mathbf{v}_t$  for all fluid phases can then be expressed as

$$\mathbf{v}_t = -\lambda_t \cdot \nabla p - \frac{1}{2} [\lambda_n - \lambda_w] \nabla p_c + \mathbf{g} [\lambda_n \rho_n + \lambda_w \rho_w]. \quad (3)$$

In these equations the subscript  $w$  refers to the wetting phase and  $n$  to the non-wetting phase, and  $t$  to the total for both phases. Here  $\rho$  denotes density of the appropriate phase,  $\lambda$  is the mobility,  $Q$  is the phase volume source or sink,  $\mathbf{g}$  is the acceleration due to gravity,  $\phi$  is the porosity of the media, and  $c$  is the compressibility of the phases.

In equations (2) and (3), the average fluid pressure  $p$  is given by

$$p = \frac{p_w + p_n}{2} \quad (4)$$

and the difference of fluid pressures of the two phases, the capillary pressure  $p_c$  given by

$$p_c = p_n - p_w. \quad (5)$$

The essentially hyperbolic equation describing the propagation of the fluids (here and in the following written for the wetting phase) in the reservoir is given by

$$\phi \frac{\partial S_w}{\partial t} = -\nabla \cdot [f_w (\mathbf{v}_t + \lambda_n (\rho_w - \rho_n) \mathbf{g})] + \nabla \cdot [\lambda_n f_w \nabla p_c] + Q_w \quad (6)$$

where  $f_w$  denotes the fractional flow function for the wetting phase.

The capillary pressure is usually small compared to the fluid pressure gradient on the reservoir scale [9]. For this reason, in the rest of this paper we neglect capillary effects.

## 3 Numerical Method

The CEVM numerical method combines a finite volume method to calculate the mass balance of the fluid phases while the fluid pressure field is computed implicitly using the finite element method. Our method for the fluid pressure field

calculation is described in [17]. Here we only describe the calculation of the mass balance via the finite volume method.

The element velocities given by the fluid pressure field and the relation defined in Equation (3) can be employed in the finite volume method to compute the mass balance for the fluid phases (Equation 6) explicitly. The finite volumes are centered around the nodes of the finite elements (Figure 1). Using the finite volume technique, neglecting capillary effects, integrating Equation (6) over an arbitrary volume  $V_i$  and applying the divergence theorem yields

$$\int_{V_i} \frac{\partial S_w}{\partial t} dV_i = - \int_{V_i} (f_w [\mathbf{v}_t + \lambda_n (\rho_n - \rho_w) \mathbf{g}]) dV_i + \int_{V_i} Q_w dV_i \quad (7)$$

Within each finite volume  $V_i$ ,  $S_w$  is constant. Discretizations of Equation (7) using Euler's method leads to

$$S_{wi}^{k+1} = S_{wi}^k - \frac{\Delta t}{\phi_i A_i} \sum_j^{n_s} (f_{wj} [\mathbf{v}_{tj} + \lambda_{nj} (\rho_{nj} - \rho_{wj}) \mathbf{g}]) \cdot \mathbf{n}_j \quad (8)$$

where  $\sum_j^{n_s}$  is the summation over all segments  $j$  belonging to the finite volume  $V_i$ ,  $\Delta t$  is the time-step,  $A_i$  is the area of the control volume,  $\mathbf{n}_j$  is the outward normal vector to segment  $j$ .

### 3.1 Second-order Accuracy and Slope Limiters

Equation (8) is solved in a fully upwind formulation. Using a first-order accurate approximation,  $S_{wi}$  is constant across volume  $i$ . First-order accuracy, however, leads to diffuse and non-physical interfaces between the fluid phases. Hence, a higher-order accurate approximation is needed.

Second-order accuracy can be achieved by computing a gradient of the saturation  $\tilde{S}_{wi}$  in the control volume  $V_i$  by using the least squares method to fit a plane through  $S_{wi}$  and the saturation values  $S_{wj}$  at the  $n$  control volumes  $V_j$  that are neighbours of  $V_i$ , such that  $S_{wi}$  varies linearly in  $V_i$ . In two dimensions, the gradient  $\mathbf{a}$  satisfies

$$M\mathbf{a} = \mathbf{b}$$

where

$$M_{kl} = \sum_{j=1}^n (x_j^k - x_i^k)(x_j^l - x_i^l) \quad \text{and} \quad \mathbf{b}_k = \sum_{j=1}^n (S_{wj} - S_{wi})(x_j^k - x_i^k)$$

where  $x_i^1$  and  $x_i^2$  are the two-dimensional spatial coordinates of the centre of mass of finite volume  $V_i$ , and  $x_j^1$  and  $x_j^2$  are the spatial coordinates of the centre of mass

of the neighbouring finite volumes  $V_j$ . Applying the gradient  $\mathbf{a}$ , the saturation  $\tilde{S}_{wj}$  in the finite volume  $V_i$  can be computed as

$$\tilde{S}_{wi}(\mathbf{x}) = S_{wi} + \mathbf{a} \cdot (\mathbf{x} - \mathbf{x}_i) \quad (9)$$

where  $\mathbf{x} \in V_i$ . Using  $\tilde{S}_{wi}$ , a relation for the relative permeability, the mobility and the fractional flow can be computed at the respective boundary segments of the finite volume, and the finite volume formulation, equation (8) can now be solved with second-order accuracy.

Although second-order accuracy is now achieved, it is essential to employ a slope limiter to avoid spurious oscillations. In particular the limited function  $\bar{S}_{wi}$  is obtained as

$$\bar{S}_{wi}(\mathbf{x}) = S_{wi} + \Psi_i (\mathbf{a} \cdot (\mathbf{x} - \mathbf{x}_i)) \quad (10)$$

where  $0 \leq \Psi_i \leq 1$  is a chosen limiter. With  $\Psi_i = 0$ , the saturation  $S_{wi}$  is constant in  $V_i$  resulting in a first-order scheme.

We use the MINIMOD limiter  $\Psi_j$  given by

$$\Psi_j = \min [r_i, 1] \quad (11)$$

where

$$r_i = \begin{cases} (S_{wi}^{\max} - S_{wi}) / (S_{wj} - S_{wi}) & \text{if } S_{wj} > S_{wi} \\ (S_{wi}^{\min} - S_{wi}) / (S_{wj} - S_{wi}) & \text{if } S_{wj} < S_{wi} \\ 1 & \text{if } S_{wj} = S_{wi} \end{cases}$$

and

$$S_{wi}^{\min} = \min(S_{wi}, S_{wn}), \quad S_{wi}^{\max} = \max(S_{wi}, S_{wn})$$

over all  $S_{wn}$  corresponding to finite volumes  $V_n$  neighbouring  $V_i$ .

## 4 Numerical Experiment: Two-phase Flow in a Fractured Reservoir

Faults in oil reservoirs have a strong influence on the total permeability of the reservoir and cause difficulties when predicting oil recovery [13], [14].

In the following a numerical experiment is provided to test the applicability of our method to reservoir simulations. The fracture is 10 cm wide and is represented as a thin cut in a planview section of the reservoir. The oil has a density of  $\rho_n = 800.0 \text{ kg m}^{-3}$  and a viscosity of  $\mu_n = 5.0 \times 10^{-3} \text{ Pa s}^{-1}$ . The water, which fills the rest of the pore space, has a density of  $\rho_w = 1000.0 \text{ kg m}^{-3}$  and a viscosity of  $\mu_w = 1.0 \times 10^{-3} \text{ Pa s}^{-1}$ . The matrix permeability in the reservoir is set to  $\mathbf{k}_f = 1.0 \times 10^{-13} \text{ m}^2$  while the fracture permeability is  $\mathbf{k}_m = 1.0 \times 10^{-09} \text{ m}^2$ .

The matrix porosity is  $\phi_m = 0.1$  while the fracture porosity is  $\phi_f = 1.0$ . The oil saturation is  $S_n = 0.9$  in the reservoir and  $S_n = 0.0$  elsewhere. The water saturation is  $S_n = 0.1$  in the reservoir and  $S_n = 1.0$  elsewhere. The well is 20 cm in diameter and its casing has a permeability of  $k_w = 1.0 \times 10^{-10} \text{ m}^2$ . The pumping rate is  $1.16 \times 10^{-4} \text{ m}^3 \text{ s}^{-1}$ . This rate leads to steep pressure gradients such that capillary effects can be neglected.

The following relative permeability relations are used in the simulations

$$k_{rw}(S_n) = 1.0 - 2.7674S_n + 2.692S_n^2 - 0.9381S_n^3$$

and

$$k_{rn}(S_n) = 1.8038S_n - 2.0551S_n^2 + 1.243S_n^3$$

which are least square fits through relative permeability values that were measured in experiments. Golder Associates ([www.golder.com](http://www.golder.com)) provided the data to us. Our numerical methods are implemented in the object-oriented C++ code CSP3D3.0 [15].

To study the effects of buoyancy forces a well with 2 m open casing is located above an inclined fracture (Figure 2) is considered. The oil reservoir is located underneath the fracture. The saturation at the bottom of the oil reservoir are held constant implying that the oil reservoir extends across the model boundaries. The model dimensions are  $100 \times 80$  metres. The unstructured mesh consisted of 9544 finite elements and 4875 finite volumes (8 MB storage requirements for the grids, CPU time on a standard 667 Mhz Pentium III is 8.5 minutes to simulate 10 days of pumping).

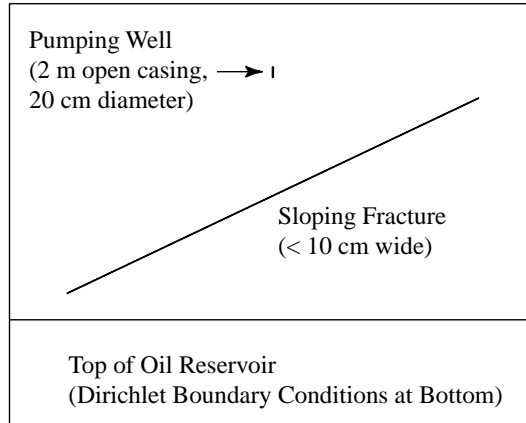


Figure 2: Model setup (cross section) for the simulation of pumping of an oil reservoir with an thin, inclined, and highly permeable fracture above the reservoir. Model dimensions are  $100 \times 80$  metres.

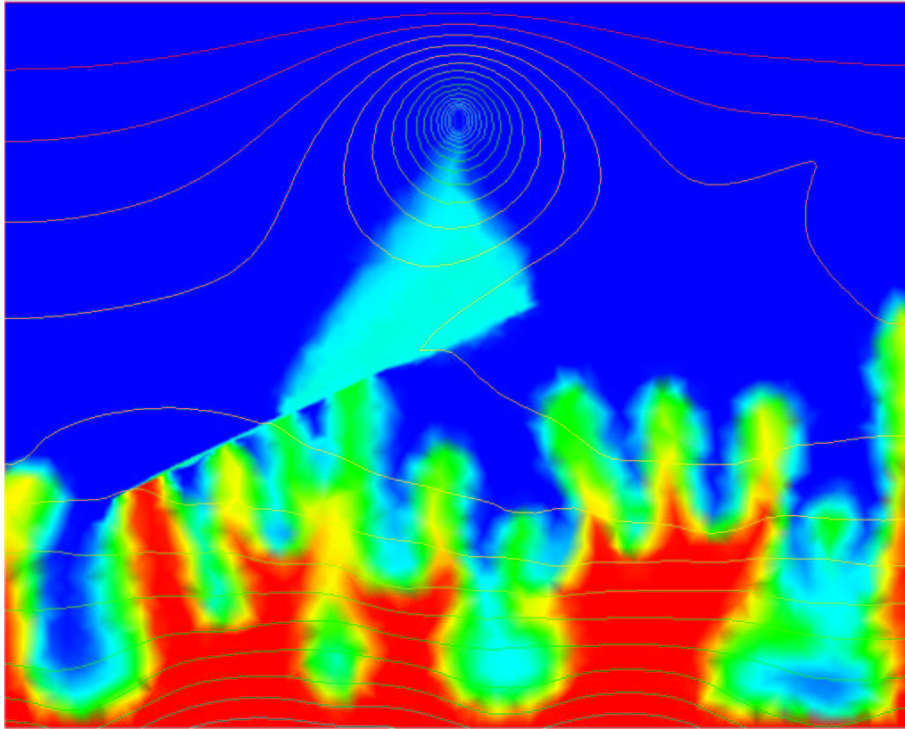


Figure 3: Oil saturation (volume fraction) after 2000 days of pumping. Oil saturation is shown in rainbow colour shading (red = 0.9, blue = 0.0). Contours depict the relative fluid pressure (with buoyancy effects). Note how the fracture and the buoyancy effects disturb the fluid pressure field. The oil is then forced into the high permeable fracture from which it progresses towards the well.

The numerical simulation (Figure 3) shows how the inclined fracture disturbs the fluid pressure gradient caused by the pumping. The fluid pressure gradient underneath the fracture is reduced, which forces the oil to rise upwards in distinct fingers. In between the fingers, the denser water sinks down into the oil reservoir. Those oil fingers, which are displacing the water, are due to the buoyancy effects, because the difference in the fluid densities imposes a stronger fluid pressure gradient underneath the fracture than the pumping. Neglecting buoyancy, the oil would still rise upwards rather uniformly. When the oil reaches the high-permeability fracture, it is drawn into the fracture from which it departs into the well. Figure 3 shows the oil saturation and relative fluid pressure after 2000 days. The total velocity  $\mathbf{v}_t$  varies from  $3.6 \times 10^{-12} \text{ m s}^{-1}$  to  $4.6 \times 10^{-5} \text{ m s}^{-1}$ .

## 5 Conclusion and Outlook

We have combined a finite element-finite volume method with node-centred finite volumes constructed on a triangular finite element grid in an implicit pressure explicit saturation approach. This was founded to be an efficient approach to model two-phase flow of incompressible fluids in geologic media with complex geometrical structures and large variations in the hydrological rock properties (permeability, porosity) and velocities. Using higher-order finite volume methods, very accurate numerical solutions can be achieved. Furthermore, the node-centred finite volumes do not require the use of a mixed-element formulation to solve for the fluid pressure and fluid velocities simultaneously. Thus, the method can deal with discontinuous changes of the material properties. Furthermore, the construction of large global matrices is avoided, which partly compensates for the storage required by the construction of the finite volume subgrid. However, the storage necessary to construct a 3D finite volume subgrid from tetrahedral elements significantly increases making the method less efficient for 3D simulations.

The proposed method is being extended to model the flow of compressible fluids and to include an equation of state to simulate the flow of miscible fluids (e.g., water and steam) in a variety of geological environments. Capillary pressure relationships will also be included such that capillary effects can be modelled accurately.

## References

- [1] Ambrosi, D., Corti, S., Pennati, V., and Saleri, F., Numerical simulation of unsteady flow at Po River delta. *Journal of Hydraulic Engineering*, **122**, 735-743, 1996.
- [2] Aziz, K. and Settari, A., Petroleum Reservoir Simulation. *Applied Science Publishers*, 476 pages, 1979.
- [3] Bergamaschi, L., Mantica, S., and Manzini, G., A mixed finite element-finite volume formulation of the black-oil model. *SIAM Journal on Scientific Computing*, **20**, 970-997, 1996
- [4] Boris, J.P. and Book, D.L., Flux-corrected transport. I. SHASTA, A fluid transport algorithm that works. *Journal of Computational Physics*, **11**, 38-69, 1973.
- [5] Durlofsky, L.J., A triangle based mixed finite-element-finite volume technique for modeling two phase flow through porous media. *Journal of Computational Physics*, **105**, 252-266, 1993.

- [6] Eymard, R., Gallouët, T., and Joly, P., Hybrid finite element techniques for oil recovery simulation. *Computer Methods in Applied Mechanics and Engineering*, **74**, 83-98, 1989.
- [7] Harten, A., ENO schemes with subcell resolution. *Journal of Computational Physics*, **83**, 148-184, 1987.
- [8] Helmig, R., Multi-phase flow and transport processes in the subsurface. *Springer Verlag*, 397 pages, 1997.
- [9] Huber, R. and Helmig, R., Multi-phase flow in heterogeneous porous media: A classical finite element method versus an implicit pressure-explicit saturation-based mixed finite element-finite volume approach. *International Journal for Numerical Methods in Fluids*, **29**, 899-920, 1999.
- [10] Huber, R. and Helmig, R., Node-centered finite volume discretizations for the numerical simulation of multi-phase flow in heterogeneous porous media. *Computational Geosciences*, **4**, 141-164, 2001.
- [11] Ingebritsen, S.E. and Sanford, W.E., Groundwater in Geologic Processes, *Cambridge University Press*, 270 pages, 1999.
- [12] Jiang, G.S. and Tadmor, E., Non-oscillatory central schemes for multidimensional hyperbolic conservation laws. *SIAM Journal on Scientific Computing*, **18**, 1892-1917, 1998.
- [13] Matthäi, S.K., and Roberts, S.G., The influence of fault permeability on single phase fluid flow near fault-sand intersections: Results from steady state high-resolution models of pressure-driven fluid flow. *American Association of Petroleum Geologists Bulletin*, **80**, 1763-1779, 1996.
- [14] Matthäi, S.K., Aydin, A., Pollard, D.D., and Roberts, S.G., Numerical simulation of departures from radial drawdown in a faulted sandstone reservoir with joints and deformation bands. In: Jones, G., Fisher, Q.J., and Knipe, R.J., (eds) *Faulting, Fault Sealing and Fluid Flow in Hydrocarbon Reservoirs*. Geological Society, London, Special Publications, **147**, 157-191, 1998.
- [15] Matthäi, S.K., Geiger, S., and Roberts, S.G., Complex System Platform CSP3D3.0 User's Guide. *Department of Earthsciences, ETH Zurich, Switzerland*, 144 pages, 2001.
- [16] Nessyahu, H. and Tadmor, E., Non-oscillatory central differencing for hyperbolic conservation laws. *Journal of Computational Physics*, **87**, 408-463, 1988.

- [17] Roberts, S. and Matthäi, S.K., High resolution potential flow methods for oil exploration. *Mathematics Research Report, The Australian National University, Centre for Mathematics and its Applications*, **MRR 003-96**, 9 pages, 1996.
- [18] Roe, P.L., Approximate Riemann solvers, parameters vectors, and difference schemes. *Journal of Computational Physics*, **43**, 357-372, 1981.
- [19] Pain, C.C., Mansoorzadeh, C.R., de Oliveira, E., and Goddard, A.J.H., Numerical modelling of gas-solid fluidized beds using the two-fluid approach. *International Journal for Numerical Methods in Fluids*, **36**, 91-124, 2001.
- [20] Shu, C.W. and Harten, A., Efficient implementation of essentially non-oscillatory shock capturing schemes. *Journal of Computational Physics*, **77**, 439-471, 1988.
- [21] Sweby, P.K., High resolution schemes using flux limiters for hyperbolic conservation laws. *SIAM Journal on Numerical Analysis*, **21**, 995-1011, 1984.
- [22] Toro, E.F., A weighted average flux method for hyperbolic conservation laws. *Proceedings of the Royal Society, Series A* **423**, 401-418, 1989.
- [23] Verma, S.K., Flexible Grids for Reservoir Simulation. *Ph.D. Thesis Stanford University*, 255 pages, 1996.
- [24] Zienkiewicz, O.C. and Taylor, R.L., The finite element method, 5th Edition. *Butterworth-Heinemann*, Volumes 1-3, 2000.
- [25] Zoppou, C. and Roberts, S., Numerical solution of the two-dimensional unsteady dam break. *Applied Mathematical Modelling*, **24**, 457-475, 2000.